Available online at www.sciencedirect.com
SCIENCE DIRECT®
Journal of Solid State Chemistry 177 (2004) 4655–4664
JOURNAL OF SOLID STATE CHEMISTRY
www.elsevier.com/locate/jssc

The structural phase transitions of aminoguanidinium(1+) dihydrogen phosphate—study of crystal structures, vibrational spectra and thermal behavior

Ivan Němec[a,*], Zorka Macháčková[a], Karel Teubner[a], Ivana Císařová[a], Přemysl Vaněk[b], Zdeněk Mička[a]

[a] *Faculty of Science, Department of Inorganic Chemistry, Charles University in Prague, Hlavova 2030, 128 40 Prague 2, Czech Republic*
[b] *Institute of Physics, The Academy of Sciences of the Czech Republic, Na Slovance 2, 182 21 Prague 8, Czech Republic*

Received 11 February 2004; received in revised form 28 July 2004; accepted 6 August 2004

Abstract

Aminoguanidinium(1+) dihydrogen phosphate was prepared by crystallization from aqueous solution. On the basis of the results of DSC measurements, X-ray structural analysis was carried out at temperatures of 160, 215 and 293 K for three aminoguanidinium(1+) dihydrogen phosphate phases (**I**|>222 K|$P\bar{1}(2)$ |$Z=2$|non-ferroic |melting point 408 K; **II** |201–222 K|$P\bar{1}(2)$ |$Z=2$|non-ferroic|-; **III** |<201 K|$P\bar{1}(2)|Z=4$|non-ferroic|-). The triclinic unit cell dimensions ($a=6.8220(2)$, $b=7.1000(2)$, $c=7.4500(2)$ Å, $\alpha=86.925(2)^\circ$, $\beta=80.731(2)^\circ$, $\gamma=79.630(2)^\circ$, $V=350.21(2)$ Å^3—phase **I**) are similar for all three structural phases with the exception of phase **III**, where doubling of the *c*-axis length leads to an increase in the volume to 692.34(3) Å^3. The crystal structure of all three modifications consists of parallel layers of dihydrogen phosphate anions that are interconnected by aminoguanidinium(1+) cations through hydrogen bonds of the N–H…O type. The planar aminoguanidinium(1+) cations are oriented almost parallel to each other and are perpendicular to the anion layers. The primary differences amongst phases **I**, **II** and **III** lie in the location of the H atom in the short O–H…O bonds connecting the dihydrogen phosphate anions in layers. The FTIR and FT Raman spectra of natural and deuterated compounds were recorded and interpreted. The FTIR spectra were studied down to a temperature of 90 K.

Keywords: Aminoguanidinium(1+) dihydrogen phosphate; Phase transition; Crystal structure; Hydrogen bonds; Vibrational spectra; Thermal behavior

1. Introduction

Intensive study of aminoguanidine and some of its salts by computational and experimental techniques [1–3] was primarily motivated by its pharmacological use. Nonetheless, similar to guanidine, aminoguanidine and its salts are also very interesting from the standpoint of preparation and study of new materials with important physical properties. For example, aminoguanidinium(1+) nitrate [4] was prepared as part of a program aimed at synthesizing new optical materials with significant birefringence. A detailed study was also carried out of a family of technically interesting compounds, consisting in aminoguanidinium fluorozirconates [5–7], of which the most interesting compound is probably aminoguanidinium(2+) hexafluorozirconate [8], a new ferroelectric material possessing piezoelectric, pyroelectric and second harmonic generation (SHG) properties.

The first information related to the crystal structure of the compound of aminoguanidine with phosphoric acid, called aminoguanidinium dihydrogen orthophosphate by the author, was published in 1977 [9]. The key role of

*Corresponding author. Fax: +420221951253.
E-mail address: agnemec@natur.cuni.cz (I. Němec).

0022-4596/$ - see front matter © 2004 Elsevier Inc. All rights reserved.
doi:10.1016/j.jssc.2004.08.010

hydrogen bonds (especially the short O–H…O type) in the crystal structure was already apparent in this work, although the positions of all the hydrogen atoms were only calculated because of the state of the art at that time.

This work, which is part of our project dealing with the preparation and study of new optical materials for SHG based on the salts of polarizable nitrogen-containing organic cations with inorganic oxo-acids, is concerned with a detailed study of the three discovered crystallographic modifications of aminoguanidinium(1+) dihydrogen phosphate (*AMGDP*) using methods of X-ray structural analysis, vibrational spectroscopy and DSC.

2. Experimental

Crystals of AMGDP were prepared by slow spontaneous evaporation of a solution obtained by dissolving of aminoguanidine hydrogencarbonate (98.5%, Aldrich) in phosphoric acid (p.a., Lachema, 2 mol dm^{-3}) in equimolar ratio at laboratory temperature. The colorless crystals obtained were collected under vacuum on an S3 frit, washed with small amount of ethanol and dried in a desiccator over KOH. Elemental analysis results for C, H and N (8.0% C, 5.2% H, 31.3% N) agree with theoretical content (7.0% C, 5.3% H, 32.6% N).

The deuterated compound was prepared by repeated recrystallization of natural compound from D_2O (99%) in a desiccator over KOH.

The X-ray data collection for the AMGDP single crystal was carried out on a Nonius Kappa CCD diffractometer (Mo$K\alpha$ radiation, graphite monochromator). The temperature of the crystal was controlled by an Oxford Cryosystems liquid nitrogen Cryostream Cooler. The phase problem was solved by direct methods (SIR-92 [10]) and the non-hydrogen atoms were refined anisotropically, using the full-matrix least-squares procedure (SHELXL-97 [11]). The H atom positions were localized on difference Fourier maps and their displacement factors were refined isotropically. The disordered hydrogen H3 in phase **II** was also found on difference Fourier map, however during refinement was moved too close to oxygen O3 (O3–H3 distance was 0.76 Å), therefore the original distance was kept and the riding model on parent oxygen was applied for the refinement. The basic crystallographic data and the details of the measurement and refinement are summarized in Table 1. Crystallographic data (excluding structure factors) for the **III**, **II** and **I** AMGDP phases have been deposited with the Cambridge Crystallographic Data Center as supplementary publications CCDC 197708, CCDC 197709 and CCDC 197710, respectively. Copies of the data can be obtained free of charge on application to CCDC, 12 Union Road, Cambridge CB21 EZ, UK (fax: (44) 1223-336-033; e-mail: deposit@ccdc.cam.ac.uk).

The infrared spectra of nujol and fluorolube mulls were recorded on a Nicolet Magna 760 FTIR spectrometer with 2 cm^{-1} resolution (4 cm^{-1} resolution in FAR IR region) and Happ-Genzel appodization in the 85–4000 cm^{-1} region (deuterated compound was measured in the 400–4000 cm^{-1} range). Low-temperature measurements were carried out by the nujol mull method in low-temperature cell with KBr or PE windows in the 298–90 K interval. The temperature was controlled by a Fe-Const. thermocouple. The analog signal was processed on a PC using the AX5232 temperature measurement board.

The Raman spectrum of polycrystalline sample was recorded on a Bruker Equinox 55/S FTIR spectrometer with a FRA 106/S Raman module (2 cm^{-1} resolution, Blackman-Harris 4-Term apodization, 1064 nm NdYAG laser excitation, 200 mW power at the sample) in the 100–4000 cm^{-1} region.

The DSC measurements were carried out on a Perkin Elmer Pyris Diamond DSC and DSC 7 instruments in the 95–375 K temperature region (nitrogen atmosphere—20 ml/min). A heating rate of 10 K/min was selected to measure approximately 10 mg of finely ground sample placed in hermetically sealed aluminum pans.

3. Results and discussion

3.1. Crystal structures

The crystal structures of all three AMGDP modifications consist of parallel layers of dihydrogen phosphate anions lying in the *ac* plane (the distance between the layers is almost equal to unit-cell parameter *b*), which are interconnected by aminoguanidinium(1+) cations through hydrogen bonds of the N–H…O type (see Fig. 1). The length of these hydrogen bonds (see Table 3) attains values in the intervals 2.826(2)–3.425(2) Å (phase **III**), 2.831(2)–3.467(2) Å (phase **II**) and 2.840(2)–3.491(2) Å (phase **I**). The extremely long donor–acceptor distances of the weakest N–H…O interactions are connected with the presence of bifurcated (three-center) hydrogen bonds to hydrogen atom H4A (phases **I** and **II**) or H14B (phase **III**) (see Table 3). A weak hydrogen bond of the N–H…N type (N24…N14 distance equal to 3.227(2) Å) interconnecting the neighboring cations was also found in phase **III**. As is apparent from Fig. 1, aminoguanidinium(1+) cations are mutually oriented almost parallel in the structure (the deviation from an ideal parallel arrangement, e.g., is equal to 2.30(2)° in phase **III**), and they are ordered perpendicular to the anion layers.

Table 1
Basic crystallographic data, data collection, and refinement parameters of AMGDP phases

	Phase **I**	Phase **II**	Phase **III**
Empirical formula		$CH_9N_4O_4P$	
Formula weight ($g\,mol^{-1}$)		172.09	
Temperature (K)	293(2)	215(2)	160(2)
Wavelength (Å)		0.71069	
Crystal system		Triclinic	
Space group		$P\bar{1}$	
a (Å)	6.8220(2)	6.8050(3)	6.7860(1)
b (Å)	7.1000(2)	7.0580(2)	7.4310(2)
c (Å)	7.4500(2)	7.4400(3)	14.1070(3)
α (°)	86.925(2)	87.169(3)	87.324(1)
β (°)	80.731(2)	80.687(3)	80.482(1)
γ (°)	79.630(2)	80.134(2)	80.769(2)
Volume ($Å^3$)	350.21(2)	347.33(2)	692.34(3)
Z	2	2	4
Calculated density ($g\,cm^{-3}$)	1.632	1.646	1.651
Absorption coeff. (mm^{-1})	0.363	0.366	0.367
$F(000)$	180	180	360
Crystal size (mm)	$0.10\times0.27\times0.20$	$0.30\times0.25\times0.10$	$0.10\times0.27\times0.20$
θ range for data collection	3.07–27.56°	2.93–27.50°	2.93–27.57°
Range of h, k and l	$0\to8$, $-8\to9$, $-9\to9$	$0\to8$, $-8\to9$, $-9\to9$	$0\to8$, $-9\to9$, $-17\to18$
Reflection collected/unique (R_{int})	3050/1598 (0.0112)	2458/1572 (0.0161)	6238/3173 (0.0137)
Phase problem solution		Direct methods	
Refinement method		Full-matrix least-squares on F^2	
Data/restrains/parameters	1598/0/126	1572/0/128	3173/0/253
Goodness-of-fit on F^2	1.065	1.132	1.053
R, wR_2 [$I>2\sigma(I)$]	0.0305, 0.0819	0.0296, 0.0776	0.0293, 0.0843
R, wR_2 (all data)	0.0325, 0.0836	0.0330, 0.0804	0.0356, 0.0888
Extinction coefficient	0.24(2)	—	—
Largest max. and min. on final $\Delta\rho$ map ($e\,A^{-3}$)	0.307 and −0.289	0.206 and −0.389	0.249 and −0.478
No. and θ range for unit-cell determination	4744, 1–27.48°	2686, 1–27.48°	10044, 1–27.48°
Scan technique		ω scan to fill Ewald sphere	
Function minimized		$[\Sigma(w(F_o^2-F_c^2))^2/\Sigma(w(F_o^2)^2]^{1/2}$	
Weighting scheme		$w^{-1}=\sigma^2(F_o^2)+(aP)^2+bP$	
	$a=0.0402$, $b=0.1083$	$a=0.0301$, $b=0.1388$	$a=0.0476$, $b=0.1701$
		$P=(F_o^2+2F_c^2)/3$	

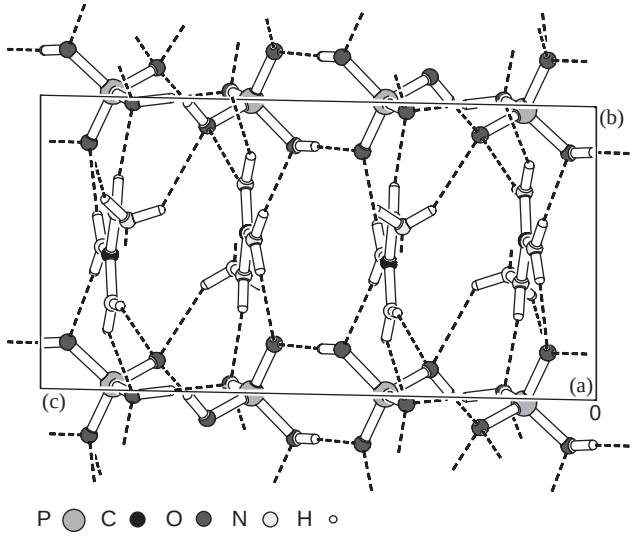

Fig. 1. Packing scheme of AMGDP phase **III** (projection to *bc* plane, dashed lines indicate hydrogen bonds).

In the cations of all the phases, non-hydrogen atoms form an almost ideal plane with deviation of an atom from the plane of about 0.02 Å. The geometry of the cations is retained in all the crystallographic modifications and the bonding distances and the angles (see Table 2) are similar to those found in other aminoguanidinium(1+) compounds [1,4]. The numbering of the individual atoms is depicted in Figs. 2 and 3.

The actual mechanism found for the **I→II→III** phase transitions is based on a change in the positions of the hydrogen atoms in short hydrogen bonds of the O–H…O type connecting the dihydrogen phosphate anions (see Fig. 4) in the layers described above. These changes are also closely connected with minor changes in the position of the oxygen atoms, which depend on the donor/acceptor role of the particular oxygen atom in the hydrogen bond network (see Tables 2 and 3).

In the low-temperature phase **III**, the anions are connected through asymmetric hydrogen bonds with a

Table 2
Selected bond lengths (Å) and angles (deg) for AMGDP phases

	Phase **I**	Phase **II**		Phase **III**		
P(1)–O(1)	1.555(1)	1.562(1)	P(1)–O(11)	1.566(1)	P(2)–O(21)	1.570(1)
P(1)–O(2)	1.515(1)	1.514(1)	P(1)–O(12)	1.512(1)	P(2)–O(22)	1.512(1)
P(1)–O(3)	1.522(1)	1.529(1)	P(1)–O(13)	1.514(1)	P(2)–O(23)	1.506(1)
P(1)–O(4)	1.537(1)	1.540(1)	P(1)–O(14)	1.560(1)	P(2)–O(24)	1.569(1)
C(1)–N(1)	1.319(2)	1.323(2)	C(1)–N(11)	1.324(2)	C(2)–N(21)	1.324(2)
C(1)–N(2)	1.319(2)	1.323(2)	C(1)–N(12)	1.326(2)	C(2)–N(22)	1.322(2)
C(1)–N(3)	1.330(2)	1.329(2)	C(1)–N(13)	1.331(2)	C(2)–N(23)	1.333(2)
N(3)–N(4)	1.407(2)	1.408(2)	N(13)–N(14)	1.410(2)	N(23)–N(24)	1.408(2)
O(1)–P(1)–O(2)	110.3(1)	110.2(1)	O(11)–P(1)–O(12)	110.7(1)	O(21)–P(2)–O(22)	109.6(1)
O(1)–P(1)–O(3)	107.5(1)	107.4(1)	O(11)–P(1)–O(13)	106.4(1)	O(21)–P(2)–O(23)	109.9(1)
O(1)–P(1)–O(4)	105.1(1)	104.7(1)	O(11)–P(1)–O(14)	104.4(1)	O(21)–P(2)–O(24)	102.1(1)
O(2)–P(1)–O(3)	112.4(1)	112.6(1)	O(12)–P(1)–O(13)	113.7(1)	O(22)–P(2)–O(23)	114.7(1)
O(2)–P(1)–O(4)	110.5(1)	110.9(1)	O(12)–P(1)–O(14)	110.6(1)	O(22)–P(2)–O(24)	109.1(1)
O(3)–P(1)–O(4)	110.8(1)	110.7(1)	O(13)–P(1)–O(14)	110.5(1)	O(23)–P(2)–O(24)	110.7(1)
N(1)–C(1)–N(2)	121.4(1)	121.2(1)	N(11)–C(1)–N(12)	120.9(1)	N(21)–C(2)–N(22)	121.4(1)
N(1)–C(1)–N(3)	120.1(1)	120.2(1)	N(11)–C(1)–N(13)	120.5(1)	N(21)–C(2)–N(23)	120.0(1)
N(2)–C(1)–N(3)	118.5(1)	118.7(1)	N(12)–C(1)–N(13)	118.6(1)	N(22)–C(2)–N(23)	118.6(1)
C(1)–N(3)–N(4)	119.0(1)	119.0(1)	C(1)–N(13)–N(14)	119.0(1)	C(2)–N(23)–N(24)	118.7(1)

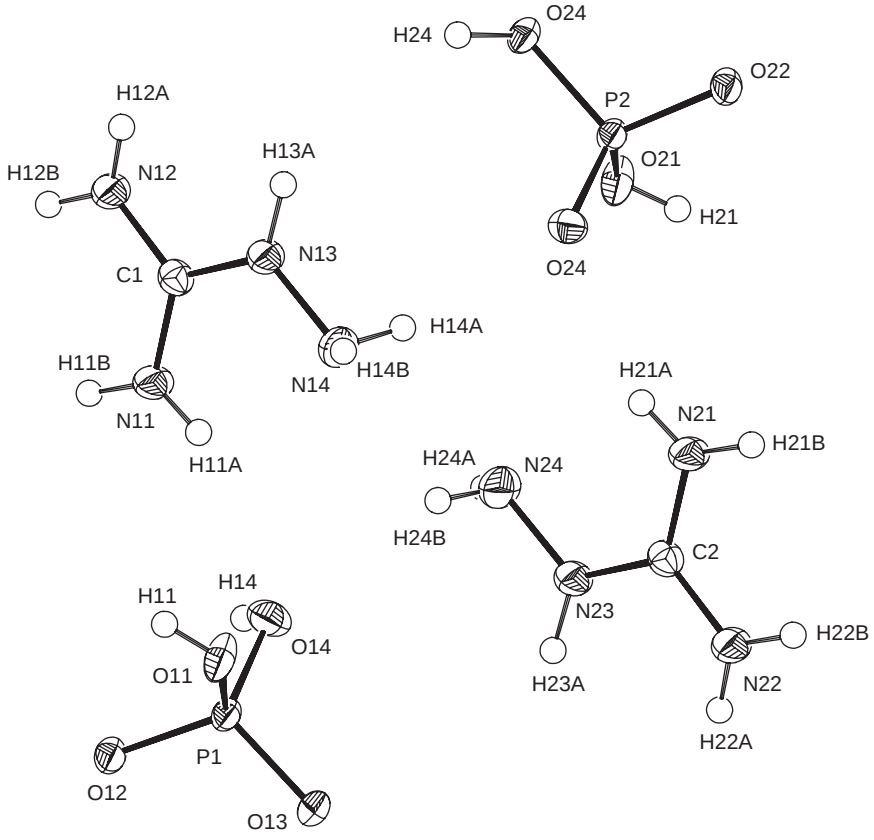

Fig. 2. Atom numbering in AMGDP phase **III**.

length of 2.512(2)–2.521(1) Å (see Table 3). The expected prolonging of the P–O(H) (1.560(1)–1.570(1) Å) bonds (i.e., P1–O11, P1–O14, P2–O21, and P2–O24) compared to the P–O (1.506(1)–1.514(1) Å) bonds (i.e., P1–O12, P1–O13, P2–O22, and P2–O23) is clearly apparent in this phase. The values of the O–P–O bonding angles vary in the range 102.1(1)–114.7(1)°. In AMGDP phase **III**, the unit-cell parameter *c* is doubled, with an increase in the number of formula units from two to four.

The other extreme, according to the H-bonding status, is crystallographic phase I (see Table 3), which is characterized by the fact that half of the H-bonds in

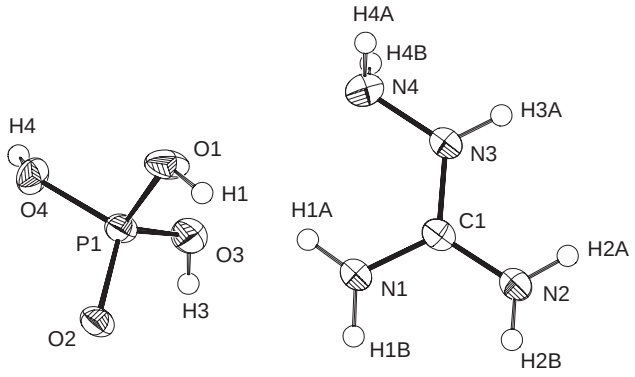

Fig. 3. Atom numbering in AMGDP phases **I** and **II**.

the dihydrogen phosphate layers are symmetric. In this modification, the asymmetric O–H…O hydrogen bond in each anion contains one oxygen atom (O2), which acts as a "classical" proton acceptor (the P1–O2 bond length equals 1.515 (1) Å) and a second one (O1), acting as a "classical" proton donor (the P1–O1 bond length equals 1.555 (1) Å). The remaining two oxygen atoms O3 and O4 (P–O bond lengths equal to 1.522(1) and 1.537(1) Å, respectively) participate in symmetric O–H–O hydrogen bonds, in which hydrogen atoms H3 and H4, lying at the crystallographic centers of symmetry, are shared between neighboring anions. The lengths of the symmetric hydrogen bonds attain values of 2.499(2) Å ($O3\ldots O3^{ii}$) and 2.498(2) Å ($O4\ldots O4^{iii}$) and the asymmetric hydrogen bond has a length of 2.504(1) Å ($O1\ldots O2^{i}$). The values of the O–P–O bonding angles vary in the range 105.1(1)–112.4(1)°.

Phase **II** is a logical transition between phases **I** and **III**. One symmetric hydrogen bond mediated by atom H4, occupying the crystallographic center of symmetry, remains unchanged (according to phase **I**) in this phase, with a length of 2.498(2) Å ($O4\ldots O4^{xi}$). The P–O(H) (i.e., P1–O4) bond has a length of 1.540(1) Å). The remaining O1, O2 and O3 atoms participate in asymmetric H-bonds, with lengths of 2.509(2) Å ($O1\ldots O2^{ix}$) and 2.496(2) Å ($O3\ldots O3^{x}$). Atom O2 acts as a proton acceptor (P1–O2 length equal to 1.514(1) Å) and atom O1 acts as a proton donor (P1–O1 length equal to 1.562(1) Å). The last O3 atom is involved in the asymmetric hydrogen bond through hydrogen H3, which has an occupation factor of 0.5. The P–O(H) (i.e., P1–O3) bond length equal to 1.529(1) Å. The values of the O–P–O bonding angles vary in the range 104.7(1)–112.6(1)°.

However, on the basis of the fact that all three structural phases crystallize in centrosymmetric space group $P\bar{1}$, the use of AMGDP as a material for SHG can be completely excluded.

3.2. Analysis of the vibrational spectra

The numbers of normal modes of the AMGDP phases were determined by extended nuclear site group analysis [12]. The results of the correlation analysis for $H_2PO_4^-$ anions internal modes are presented in Table 4.

Crystals of phase **I** belong in the $P\bar{1}(C_i^1)$ space group with 20 atoms per asymmetric unit ($Z=2$). Except of hydrogen atoms H1 and H4 occupying one-fold positions $a(C_i)$ and $d(C_i)$, respectively, all the atoms occupy two-fold positions $i(C_1)$. Two types of species present in the unit-cell, aminoguanidinium(1+) cation and $H_2PO_4^-$ anion, occupying two-fold positions $i(C_1)$, were considered in more detailed calculations of the internal and external modes. The results are the representations $12A_g(RA)+12A_u(IR)$ for external modes and $42A_g(RA)+48A_u(IR)$ for internal modes.

Crystals of phase **II** belong in the $P\bar{1}(C_i^1)$ space group with 20 atoms per asymmetric unit ($Z=2$). Except of hydrogen atom H4 occupying one-fold position $a(C_i)$, all the atoms occupy two-fold positions $i(C_1)$. Two types of species present in the unit-cell, aminoguanidinium(1+) cation and $H_2PO_4^-$ anion, occupying two-fold positions $i(C_1)$, were considered in more detailed calculations of the internal and external modes. The results are the representations $12A_g(RA)+12A_u(IR)$ for external modes and $45A_g(RA)+48A_u(IR)$ for internal modes.

Crystals of phase **III** belong in the $P\bar{1}(C_i^1)$ space group with 38 atoms per asymmetric unit ($Z=4$). All the atoms occupy two-fold positions $i(C_1)$. Four types of species present in the unit-cell, two aminoguanidinium(1+) cations and two $H_2PO_4^-$ anions, occupying two-fold positions $i(C_1)$, were considered in more detailed calculations of the internal and external modes. The results are the representations $24A_g(RA)+24A_u(IR)$ for external modes and $90A_g(RA)+90A_u(IR)$ for internal modes.

However, expected level of factor group splitting has not been observed even in low-temperature IR spectra. This fact could be explained by small inter-ion interaction in the unit-cell and also in terms of the fact that all the measurements were carried out on polycrystalline samples.

3.3. Vibrational spectra

The vibrational spectra of AMGDP are depicted in Figs. 5–7 and the wavenumbers of the maxima are given in Table 5.

On the basis of a successful computational study concerned with the molecular structure of aminoguanidine and its cations [1], the assignment of the aminoguanidinium(1+) spectral bands was based on calculation of the vibrational spectra by analogous ab initio and DFT methods (HF, MP2, B-LYP and B3-LYP; basis set 6–31 G(d) [13]) using Gaussian 98 W [14]

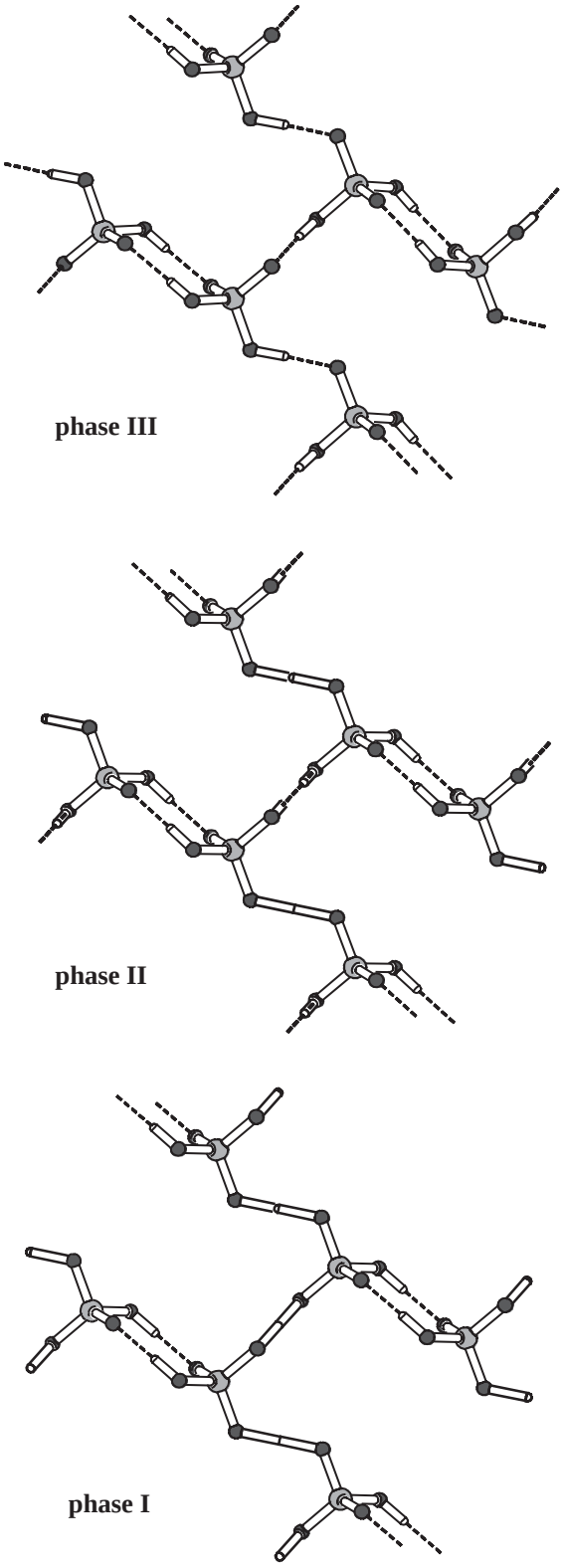

Fig. 4. Changes of H-bonding in anion layers of AMGDP phases. Dashed lines indicate asymmetric hydrogen bonds.

Table 3
Hydrogen bond lengths (Å) and angles (°) for AMGDP phases

D–H…A	d(D–H)	d(H…A)	d(D…A)	<(DHA)
Phase I				
O(1)–H(1)…O(2)^{i}	0.92(3)	1.59(3)	2.504(1)	179(3)
O(3)–H(3)…O(3)^{ii}	1.25	1.25	2.499(2)	180
O(4)–H(4)…O(4)^{iii}	1.25	1.25	2.498(2)	180
N(1)–H(1A)…O(3)	0.87(2)	2.38(2)	3.134(2)	145(2)
N(1)–H(1B)…O(4)^{iv}	0.90(2)	2.25(2)	3.093(2)	156(2)
N(2)–H(2A)…O(2)^{v}	0.89(2)	1.96(2)	2.840(2)	178(2)
N(2)–H(2B)…O(1)^{iv}	0.81(2)	2.10(2)	2.913(2)	172(2)
N(3)–H(3A)…O(4)^{v}	0.89(2)	2.08(2)	2.965(2)	170(2)
^{a}N(4)–H(4A)…O(2)^{vi}	0.92(3)	2.42(3)	3.206(2)	144(3)
^{a}N(4)–H(4A)…O(1)^{vii}	0.92(3)	2.64(3)	3.491(2)	154(3)
N(4)–H(4B)…O(3)^{viii}	0.84(3)	2.32(3)	3.099(2)	153(3)
Phase II				
O(1)–H(1)…O(2)^{ix}	0.89(3)	1.62(3)	2.509(2)	177(3)
O(3)–H(3)…O(3)^{x}	1.06	1.45	2.496(2)	169
O(4)–H(4)…O(4)^{xi}	1.25	1.25	2.498(2)	180
N(1)–H(1A)…O(3)^{xii}	0.87(2)	2.36(2)	3.107(2)	145(2)
N(1)–H(1B)…O(4)	0.89(2)	2.22(2)	3.078(2)	160(2)
N(2)–H(2A)…O(2)^{vi}	0.87(2)	1.96(2)	2.831(2)	179(2)
N(2)–H(2B)…O(1)	0.82(2)	2.09(3)	2.913(2)	172(2)
N(3)–H(3A)…O(4)^{vi}	0.89(2)	2.07(2)	2.957(2)	170(2)
^{a}N(4)–H(4A)…O(2)^{xiii}	0.95(3)	2.39(3)	3.200(2)	143(2)
^{a}N(4)–H(4A)…O(1)^{xiv}	0.95(3)	2.59(3)	3.467(2)	154(2)
N(4)–H(4B)…O(3)^{xv}	0.81(3)	2.37(3)	3.097(2)	151(3)
Phase III				
O(11)–H(11)…O(12)^{xvi}	0.78(2)	1.74(2)	2.516(1)	176(2)
O(14)–H(14)…O(23)^{xvii}	0.94(3)	1.58(3)	2.512(2)	175(2)
N(11)–H(11A)…O(14)	0.83(2)	2.40(2)	3.109(2)	145(2)
N(11)–H(11B)…O(13)^{xii}	0.90(2)	2.19(2)	3.037(2)	158(2)
N(12)–H(12A)…O(12)^{xviii}	0.84(2)	1.98(2)	2.826(2)	179(2)
N(12)–H(12B)…O(11)^{xii}	0.82(2)	2.10(2)	2.915(2)	171(2)
N(13)–H(13A)…O(13)^{xviii}	0.90(2)	2.02(2)	2.909(1)	170(2)
N(14)–H(14A)…O(23)	0.84(2)	2.29(2)	3.056(2)	153(2)
^{a}N(14)–H(14B)…O(12)^{xix}	0.91(2)	2.44(2)	3.201(2)	142(2)
^{a}N(14)–H(14B)…O(11)^{vii}	0.91(2)	2.61(2)	3.425(2)	150(2)
O(21)–H(21)…O(22)^{xx}	0.80(2)	1.72(2)	2.521(1)	177(2)
O(24)–H(24)…O(13)^{xviii}	0.97(2)	1.55(2)	2.514(1)	178(2)
N(21)–H(21A)…O(23)	0.84(2)	2.34(2)	3.068(2)	146(2)
N(21)–H(21B)…O(24)^{iv}	0.88(2)	2.28(2)	3.101(2)	156(2)
N(22)–H(22A)…O(22)^{xxi}	0.85(2)	1.98(2)	2.830(2)	177(2)
N(22)–H(22B)…O(21)^{iv}	0.82(2)	2.11(2)	2.915(2)	169(2)
N(23)–H(23A)…O(24)^{xxi}	0.90(2)	2.09(2)	2.988(1)	173(2)
N(24)–H(24A)…O(22)^{xvii}	0.91(2)	2.35(2)	3.179(2)	151(2)
^{a}N(24)–H(24B)…O(14)	0.87(2)	2.43(2)	3.125(2)	137(2)
^{a}N(24)–H(24B)…N(14)	0.87(2)	2.67(2)	3.227(2)	124(2)

Note. Equivalent positions: (i) $-x+1,-y+1,-z$; (ii) $-x+1,-y,-z$; (iii) $-x+2,-y,-z$; (iv) $x-1,y,z$; (v) $x-1,y,z+1$; (vi) $x,y,z+1$; (vii) $-x+1,-y+1,-z+1$; (viii) $-x+1,-y,-z+1$; (ix) $-x-1,-y+1,-z$; (x) $-x-1,-y,-z$; (xi) $-x,-y,-z$; (xii) $x+1,y,z$; (xiii) $x+1,y,z+1$; (xiv) $-x,-y+1,-z+1$; (xv) $-x,-y,-z+1$; (xvi) $-x+1,-y+2,-z+1$; (xvii) $x,y+1,z$; (xviii) $x+1,y-1,z$; (xix) $x,y-1,z$; (xx) $-x+1,-y,-z+2$; (xxi) $x-1,y+1,z$.Abbreviations: A—acceptor, D—donor.

[a]Bifurcated (three-centered) hydrogen bonds.

and GaussViewW 2.1 [15] software. The FTIR spectrum of deuterated AMGDP was also studied to confirm the proposed interpretation.

The broad structured band in the 3500–2950 cm^{-1} region, which is more intense in the IR spectrum, corresponds to the stretching vibrations of the NH

Table 4
Correlation diagram for the internal modes of $H_2PO_4^-$ anions in AMGDP crystals

Free PO_4 T_d	Free H_2PO_4 C_{2v}	Site group C_1	Factor group C_i
ν_1 – A_1(R)	A_1	A	A_g(R) + A_u(IR)
ν_2 – E(R)	A_1	A	A_g(R) + A_u(IR)
	A_2	A	A_g(R) + A_u(IR)
ν_3 – F_2(IR, R)	A_1	A	A_g(R) + A_u(IR)
	B_1	A	A_g(R) + A_u(IR)
	B_2	A	A_g(R) + A_u(IR)
ν_4 – F_2(IR, R)	A_1	A	A_g(R) + A_u(IR)
	B_1	A	A_g(R) + A_u(IR)
	B_2	A	A_g(R) + A_u(IR)

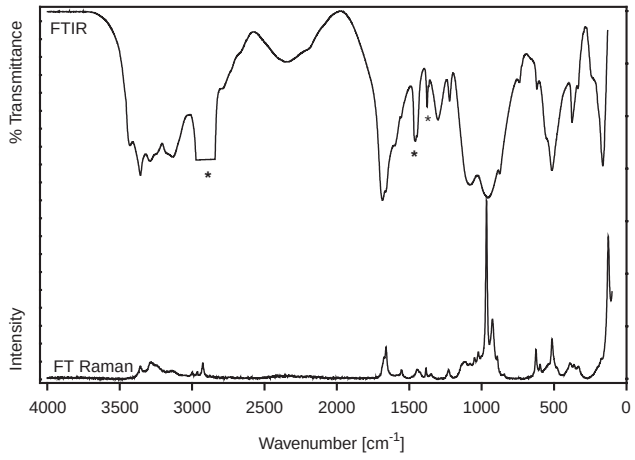

Fig. 5. FTIR (nujol mull) and FT Raman spectra of AMGDP at 298 K. Nujol bands are indicated by asterisk.

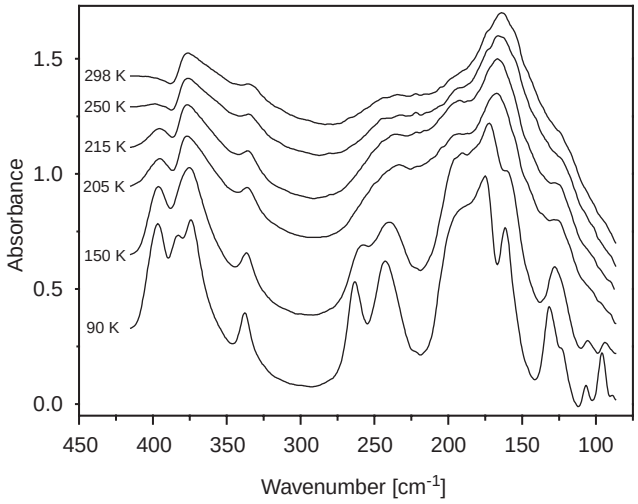

Fig. 6. FTIR (nujol mull) spectra of AMGDP at different temperatures in FAR IR region.

group participating in the hydrogen bonds of the N–H…O or N–H…N types. As expected, this band is shifted to the 2800–2600 cm^{-1} region in the spectrum of deuterated sample.

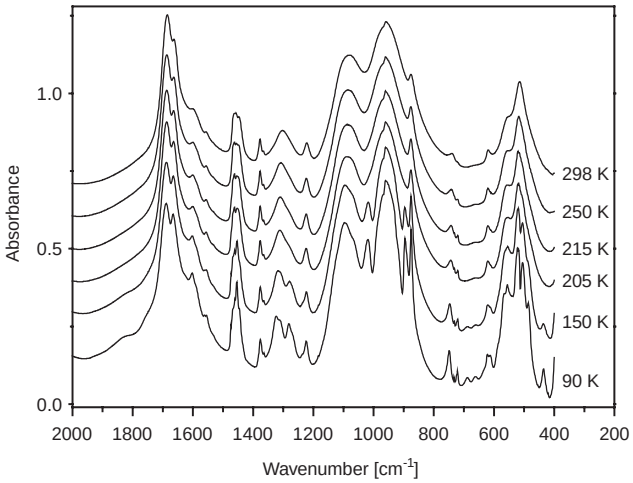

Fig. 7. FTIR (nujol mull) spectra of AMGDP at different temperatures in MID IR region.

The manifestations of stretching O–H vibrations are somewhat more complicated. Similar to a number of alkaline metal acidic phosphates [16], the existence of short O–H…O hydrogen bonds is connected with the formation of the characteristic "ABC" structure of the νO–H(…O) vibrational bands. For AMGDP, these bands can be observed only in the IR spectrum and are centered around 2780 (band A), 2345 (band B) and approx. 1650 cm^{-1} (band C). Band C is additionally overlapped by the intense vibrational manifestations of the cation (i.e., δNH_2, δNCN, δCNH and νCN vibrations).

In addition to the above-mentioned bands in the 1750–1580 cm^{-1} region, the presence of the aminoguanidinium(1+) cation is also indicated by the bands sensitive to deuteration at approx. 1555 cm^{-1}, 1445 cm^{-1} (δCNH) and approx. 1225 cm^{-1} (ρNH_2). The most intense band in the Raman spectrum at 967 cm^{-1} is very characteristic, and can be assigned to the mixed vibrations $\nu_s CN_3$, νNN and δCNH.

The vibrational manifestation of the anionic part of AMGDP is characterized in the IR spectrum by a pair of bands at 1082 and 960 cm^{-1} derived from the originally triply degenerate phosphate vibration ν_3 (see Table 4). The band of the $\nu_4 PO_4$ vibration at 515 cm^{-1} is also very intense and is also clearly visible in the Raman spectrum (514 cm^{-1}), where, next to $\nu_1 PO_4$ at 926 cm^{-1}, it is the second most intense band of the anion. The medium-intense band of POH deformation vibrations at 1304 cm^{-1} is very characteristic for acidic phosphates (the bands corresponding to the δ POD vibrations are located at 935 and 918 cm^{-1} in the spectrum of the deuterated analogue).

3.4. Thermal behavior

Crystals of AMGDP are stable in the air up to the melting point at 408 K. The DSC curves of the natural

Table 5
FTIR and FT Raman spectra (cm^{-1}) of AMGDP

IR			Raman (peak intensity)	IR deuter. sample	Assignment
298 K	215 K	90 K			
3429 m	3429 m	3430 m		3430 sh	νN–H(…O), νN–H(…N)
		3368 m		3400 m	
3358 s	3360 s	3357 s	3358(7)	3342 m	
		3335 m		3314 m	
3292 m	3294 m	3295 m	3284(10)	3295 sh	
3250 sh	3250 sh	3244 m	3250(8)		
3170 sh	3175 sh	3175 m		3191 m	
3134 m	3126 m	3123 m	3140(5)	3130 m	
		3040 m			?
		3003 m			
2865 m	n.o.[a]	n.o.		2880 wb	νO–H(…O) A band
2775 m	n.o.	n.o.		2780 wb	
				2588 m	νN–D(…O)
				2513 m	
				2443 m	
				2378 m	
				2350 m	
				2316 m	νN–D(…O), νO–D(…O)
2345 mb	2345 mb	2345 mb			νO–H(…O) B band
2210 sh	2205 sh	2205 mb			
		1820 sh			?
				1675 sh	δCNH, νCN, νO–D(…O)
1686 s	1687 s	1689 s	1675(12)		δNH_2, δCNH, νCN,
1663 s	1664 s	1666 s	1661(19)		νO–H(…O) C band
				1606 s	νCN, δNCN, νO–D(…O)
1601 m	1601 m	1603 m			ν CN, δ NCN, δ CNH,
		1562 m			νO–H(…O) C band
1557 m	1557 m	1555 m	1554(6)		δCNH, νCN
1442 m	n.o.	n.o.	1445(6)		
			1385(7)		?
				1302 m	δND_2, δCND
1304 m	1310 m	1324 m	1350(3)		δPOH
		1313 sh			
		1281 m			
				1215 sh	νNN, νCN
1222 m	1224 m	1224 w	1229(6)		ρNH_2, νNN, νCN
			1120(10)		
				1140 sh	δCND
				1167 sh	
1082 s	1087 s	1096 s	1080(9)	1100 s	ν_3PO_4
		1070 sh	1050(12)		
		1019 s	1023(16)		νCN, δCNN
970 sh	970 sh	970 sh	967(100)		$\nu_s CN_3$, νNN, δCNH
960 s	960 s	960 s		950 sh	ν_3PO_4
				935 s	δPOD
			926(34)		ν_1PO_4
				918 s	δPOD
		896 s	892(13)		γO–H(…O)
876 m	876 m	875 s			
			845(3)		?
				850 m	ρND_2
				783 m	?
739 w	743 w	749 w		735 w	γN–H(…O)
		689 w			?
		662 w			
				650 w	γO–D(…O)
620 w	620 w	622 w	625(17)		δNCN, δCNN, ρNH_2
		613 w	597(9)		
		566 m			τNH_2, γCNH
550 sh	556 m	556 m			

Table 5 (*continued*)

IR			Raman (peak intensity)	IR deuter. sample	Assignment
298 K	215 K	90 K			
				545 sh	γN–D(…O)
515 m	521 m	522 m			ν_4PO_4, τNH_2, γCNH
		518 m	514(23)		
		505 m			
				508 m	ν_4PO_4
		486 m	484(7)		τNH_2, γCNH
		436 w			?
410 sh	396 m	397 m	390 (9)		ν_2PO_4
		383 m	384(9)		
376 m	377 m	374 m	364(8)		
336 m	336 m	338 m	331(7)		δNCN, δCNN
		263 w			External modes
230 sh	236 m	243 w			
	192 m	190 sh			
164 m	167 m	175 s			
		162 s			
	128 w	132 w	126(80)		
		124 sh			
		107 w			
		96 w			

Note. Abbreviations: s, strong; m, medium; w, weak; b, broad; sh, shoulder; ν, stretching; δ, deformation or in-plane bending; γ, out-of-plane bending; ρ, rocking; τ, torsion; s, symmetric.

[a]n.o., Not observed due to nujol bands.

compound exhibit two anomalies, indicating the presence of two phase transitions (see Fig. 8). The first of these is a λ-type anomaly, with a maximum at 201 K ($\Delta c_p = 20$ J/mol K) on heating and a minimum at 199 K ($\Delta c_p = 15$ J/mol K) on cooling. The second is an S-shaped step, which is characteristic for glass transitions. This can be explained by that the phase **II** could be regarded as a dipole glass. The glass transition temperature (a midpoint) is $T_g = 222$ K ($\Delta c_p = 19$ J/mol K) on heating and $T_g = 221$ K ($\Delta c_p = 17$ J/mol K) on cooling.

Two anomalies are again present on the DSC curves of the deuterated sample. The first is an S-shaped step ($T_g = 218$ K, $\Delta c_p = 7$ J/mol K on heating), which is distinct only on heating; the low-temperature side of the step is diffuse on cooling. The second is a λ-type anomaly with a maximum at 272 K ($\Delta c_p = 9$ J/mol K) on heating and minimum at 269 K ($\Delta c_p = 8$ J/mol K) on cooling. Surprisingly, the λ-type anomaly is present at higher temperatures than the S-shaped step, in contrast to natural AMGDP.

It was observed that the history of the AMGDP sample (i.e., drying process, storage conditions, etc.) affects the intensity and even the shape of the anomalies (especially S-shaped step) on the DSC curves. All the data (i.e., T_{max}, T_{min}, T_g and Δc_p) are therefore presented as a mean values obtained from several recordings on several samples.

Changes in the FTIR spectra associated with a decrease in the sample temperature can be observed in the area of the external modes and in the bands of the

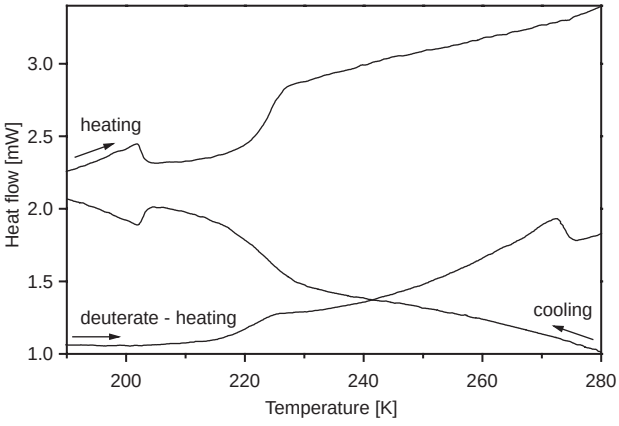

Fig. 8. DSC curves of AMGDP.

fundamental vibrations of the phosphate anions (see Figs 6 and 7).

As the temperature decreases, the maximum of the broad medium-intense band at 164 cm^{-1} shifts by 11 cm^{-1} to higher wavenumbers and the band simultaneously becomes highly split (at the lowest temperature, maxima are apparent at 132, 162, 175 and 190 cm^{-1}). The branch of this band at 230 cm^{-1} behaves similarly (shift to higher wavenumbers by 13 cm^{-1}) and finally separates into two bands at temperatures below 205 K.

The temperature effect can be observed for all the IR-active bands of the anion fundamental vibrations derived from the ν_2–ν_4 vibrations of the initial phosphate anion (see Table 4). As the temperature decreases, the asymmetrical doublet of the ν_2 vibration at 390 cm^{-1}

splits into the final triplet. A decrease in the temperature is connected with a shift in the maxima of the bands (505–522 cm^{-1} region) of the originally triply degenerate v_4 vibration by approx. 6 cm^{-1} to higher wavenumbers and also with a marked separation of the most intense band at temperatures below 205 K. Spectral changes are also apparent for the doublet (maxima at approx. 960 and 1080 cm^{-1}) of the originally triply degenerate v_3 vibration. A decrease in the sample temperature leads only to an increase in the wavenumber of the band at 1080 cm^{-1} (by as much as 14 cm^{-1}). At temperatures below 205 K, a new band appears in the spectrum at 1019 cm^{-1}, and can be assigned to manifestations of the νCN and δCNN vibrations, rather than to another branch of the v_3 vibration.

A decrease in the temperature is also clearly noticeable in the bands of the γO–H(…O) vibration (formation of an almost symmetric doublet at 896 and 875 cm^{-1} on cooling below 205 K) and the δPOH vibration (shifting to higher wavenumbers). At temperatures below 205 K, the formation of a new branch of the δ POH vibrational band at approx. 1280 cm^{-1} is also apparent.

All the observed spectral changes are completely in accord with the mechanism of studied structural phase transitions, which is characterized by the fact that, as the temperature decreases, the content of symmetric O–H…O hydrogen bonds connecting anions decreases and the content of classical asymmetric hydrogen bonds increases. This mechanism can be considered as a trend connected with a certain decrease in the symmetry of the anions, which is characteristically manifested in the spectra through splitting or separation of the bands involved in anion vibrational manifestations. However, for phase **III**, it is also necessary to consider the influence of doubling of the number of formula units.

As expected, the vibrational manifestations of the cations are practically independent of the temperature, perhaps with the exception of a certain separation of the bands of the νN–H(…O) vibrations.

Acknowledgments

This study was carried out with the financial assistance of the Grant Agency of the Czech Republic, Grant 203/01/D136, and the Grant Agency of Charles University in Prague, Grant 247/2001/B-CH, and is part of the long-term Research Plan of the Faculty of Science "Structure, Dynamics and Function of Molecular and Supramolecular Assemblies" (MSM11310001).

References

[1] J.T. Koskinen, M. Koskinen, I. Mutikainen, B. Mannfors, Z. Naturforsch. 51b (1996) 1771.
[2] M. Koskinen, I. Mutikainen, H. Elo, Z. Naturforsch. 49b (1994) 556.
[3] M. Koskinen, I. Mutikainen, P. Tilus, E. Pelttari, M. Korvela, H. Elo, Monatsh. Chem. 128 (1997) 767.
[4] A. Akella, D.A. Keszler, Acta Crystallogr. C 50 (1994) 1974.
[5] M.R. Bauer, C.R. Ross II, R.M. Nielson, S.C. Abrahams, Inorg. Chem. 38 (1999) 1028.
[6] C.R. Ross II, B.L. Paulsen, R.M. Nielson, S.C. Abrahams, Acta Crystallogr. B 54 (1998) 417.
[7] C.R. Ross II, M.R. Bauer, R.M. Nielson, S.C. Abrahams, Acta Crystallogr. B 58 (2002) 841.
[8] M.R. Bauer, D.L. Pugmire, B.L. Paulsen, R.J. Christie, D.J. Arbogast, C.S. Gallagher, W.V. Raveane, R.M. Nielson, C.R. Ross II, P. Photinos, S.C. Abrahams, J. Appl. Cryst. 34 (2001) 47.
[9] J.M. Adams, Acta Crystallogr. B 33 (1997) 1513.
[10] A. Altomare, G. Cascarano, C. Giacovazzo, A. Guagliardi, M.C. Burla, G. Polidori, M. Camalli, J. Appl. Cryst. 27 (1994) 435.
[11] G.M. Sheldrick, SHELXL-97, University of Göttingen, 1997.
[12] D.L. Rousseau, R.P. Bauman, S.P.S. Porto, J. Raman Spectrosc. 10 (1981) 253.
[13] I. Němec, Z. Macháčková, P. Vaněk, Z. Mička, J. Mol. Struct., to be published.
[14] M.J. Frisch, G.W. Trucks, H.B. Schlegel, G.E. Scuseria, M.A. Robb, J.R. Cheeseman, V.G. Zakrzewski, J.A. Montgomery Jr., R.E. Stratmann, J.C. Burant, S. Dapprich, J.M. Millam, A.D. Daniels, K.N. Kudin, M.C. Strain, O. Farkas, J. Tomasi, V. Barone, M. Cossi, R. Cammi, B. Mennucci, C. Pomelli, C. Adamo, S. Clifford, J. Ochterski, G.A. Petersson, P.Y. Ayala, Q. Cui, K. Morokuma, P. Salvador, J.J. Dannenberg, D.K. Malick, A.D. Rabuck, K. Raghavachari, J.B. Foresman, J. Cioslowski, J.V. Ortiz, A.G. Baboul, B.B. Stefanov, G. Liu, A. Liashenko, P. Piskorz, I. Komaromi, R. Gomperts, R.L. Martin, D.J. Fox, T. Keith, M.A. Al-Laham, C.Y. Peng, A. Nanayakkara, M. Challacombe, P.M.W. Gill, B. Johnson, W. Chen, M.W. Wong, J.L. Andres, C. Gonzalez, M. Head-Gordon, E.S. Replogle, J.A. Pople, Gaussian 98W (Revision A.11), Gaussian, Inc., Pittsburgh, PA, 2001.
[15] GaussViewW, version 2.1, Gaussian, Inc., Pittsburgh, PA, 2001.
[16] J. Baran, T. Lis, M. Drozd, H. Ratajczak, J. Mol. Struct. 516 (2000) 185.